Paleomagnetic Evidence for Pre-21 Ma Independent Drift of South Sardinia From North Sardinia-Corsica: "Greater Iberia" Versus Europe

Gaia Siravo[1] , **Fabio Speranza[1]** , **and Massimo Mattei[2]**

[1]Istituto Nazionale di Geofisica e Vulcanologia, Roma, Italy, [2]Dipartimento di Scienze Geologiche, Università di Roma Tre, Roma, Italy

Abstract It is unanimously acknowledged that the Corsica-Sardinia microplate rotated counterclockwise (CCW) by 40–50° between 21 and 15 Ma, synchronous with Liguro-Provençal Basin oceanic spreading. Conversely, 60–120° CCW rotations with respect to Europe from Sardinia (Permian dykes, volcanics and sediments, Mesozoic carbonates, and lower Eocene limestones) have been interpreted to be related to (a) late Permian intra-Pangea shear events, (b) Aptian Iberia rotation, and (c) Eocene Valais Ocean closure. We report paleomagnetic data from 31 red-bed sites from the mid-late Eocene (45–32 Ma) Cixerri Fm. exposed in SW Sardinia. Characteristic paleomagnetic directions from 25 dual polarity sites (240 samples) define an 86 ± 7° CCW rotation. We suggest that a S Sardinia block located NE of Balearic Islands rotated 30° CCW during the 30–21 Ma Liguro-Provençal rifting, and was decoupled from N Sardinia along the left-lateral Nuoro fault. After 21 Ma, Corsica-Sardinia underwent a drift-related 60° CCW rotation as a whole. A re-analysis of available paleomagnetic results shows that Permian data from N Sardinia-Corsica align with European directions considering a 60° CCW rotation, whereas Permian and mid Jurassic data from S Sardinia match European directions only after considering a ~35° CCW Iberia rotation besides the 90° post-Eocene event. We suggest that S Sardinia was part of Iberia, and rotated CCW during both Aptian Iberia drift and Oligo-Miocene Liguro-Provençal opening. Our data, along with recent paleomagnetic results from Calabria, suggest that S Sardinia, Balearic Islands, Calabria, Peloritan, Kabylies, and Alboran were fragments of "Greater Iberia," joined to Iberia before 30 Ma Liguro-Provençal rifting.

1. Introduction

In the Mediterranean domain, Pangea breakup, spreading of the Alpine Tethys Ocean, and collision between the irregularly shaped African and European margins occurred from late Paleozoic to early Cenozoic (Dewey et al., 1989; Le Breton et al., 2021). Additionally, subduction and fast roll-back of Alpine and Neo-Tethys Ocean slabs occurring since the mid-Cenozoic, led to the formation of a snaky Alpine chain made by a mosaic of microplates and arcuate mountain fronts (Figure 1; Alvarez et al., 1974; Faccenna et al., 2001; Jolivet et al., 2020; Malinverno & Ryan, 1986). In this frame, paleomagnetism has shown to be a valuable approach to quantify the timing and magnitude of orogenic drift events (e.g., Gattacceca et al., 2007; Maffione et al., 2013; Speranza et al., 2018), as well as to reconstruct original paleogeography and provenance of detrital deposits (Pinter et al., 2018).

Corsica-Sardinia is a fragment of Hercynian Europe that drifted away during microplate dispersal occurred at the rear of a rolling-back Alpine Tethys slab that induced opening of the Liguro-Provençal Basin, formation and migration of an Alpine orogenic salient, and Oligo-Miocene (predominantly 25–15 Ma) calk-alkaline volcanism in western Sardinia.

Both the intensely magnetized Permian and Oligo-Miocene volcanic rocks from Sardinia were paleomagnetically investigated (De Jong et al., 1969; Edel et al., 1981; Gattacceca et al., 2007; Montigny et al., 1981; Nairn & Westphal, 1968; Zijderveld et al., 1970, among many others). Paleomagnetic and $^{40}Ar/^{39}Ar$ data from the lower-mid Miocene volcanic rocks (Gattacceca et al., 2007) and sedimentary rocks (Speranza et al., 2002), indicate that Corsica-Sardinia rotated 40–50° counterclockwise (CCW) with respect to Europe after 21 Ma, synchronous with oceanic crust spreading in the Liguro-Provençal Sea, and that rotation ended around 15 Ma. A statistically indistinguishable magnitude of 60° CCW rotation in Permian dykes from NE Sardinia and S Corsica was considered as pivotal for excluding a rotational decoupling between the two continental blocks (Vigliotti et al., 1990; Figure 1).
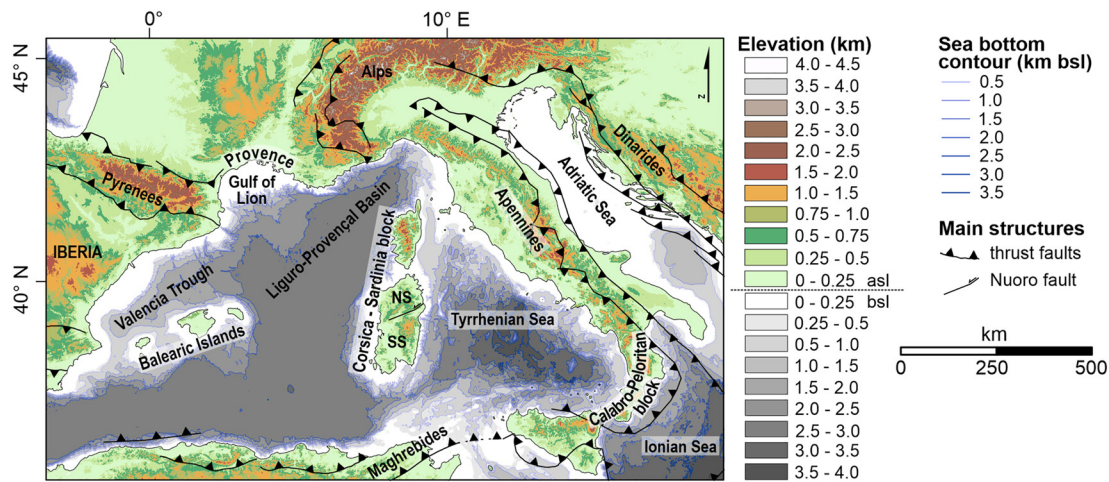
Figure 1. Geographic map and main tectonic features of the western-central Mediterranean region. SS, South Sardinia; NS, North Sardinia.

Considerably less agreement exists on the significance of larger magnitude of 90–120° CCW rotations with respect to Europe documented in S Sardinia (S of the Nuoro fault system, Figure 2a) from Permian dykes, volcanic rocks and sedimentary rocks (Aubele et al., 2014; Bachtadse et al., 2018; Edel et al., 1981), and Meso-Cenozoic carbonates (Advokaat et al., 2014; Horner & Lowrie, 1981; Kirscher et al., 2011). Aubele et al. (2014) related such inferred rotations to an intra-Pangea mega-shear zone guiding the Permian evolution from Pangea B to the classical Pangea A configuration. Kirscher et al. (2011) suggested that the 90–100° post-Jurassic CCW rotation is due to the sum of the mid-Cretaceous Iberia rotation (to which Sardinia would have been joined) during Bay of Biscay opening, and the Oligo-Miocene rotational event. Finally, Advokaat et al. (2014) reported a 95° CCW rotation from the lower Eocene Miliolitico Fm. of SW Sardinia. The 45° excess rotation with respect to the 50° occurred in the Miocene was related to an Eocene (55–30 Ma) rotational closure of the Valais Ocean and incorporation of the Briançonnais terrain into the Alps. Consequently, Advokaat et al. (2014) dismissed the hypothesis of a connection between Iberia and Sardinia and their synchronous mid Cretaceous rotation.

Here we show that SW Sardinia underwent a post-late Eocene ~90° CCW rotation that we relate to the independent kinematics of a S Sardinia block during the 30–21 Ma rifting of the Liguro-Provençal basin. The re-evaluation of previous paleomagnetic data using stringent statistical criteria also suggests that S Sardinia was previously part of Iberia and therefore participated to its Early-mid Cretaceous rotation.

2. Geologic Setting

The Hercynian chain rocks of Sardinia were intruded by late Carboniferous-early Permian granitic plutons cut in turn by early -mid Permian dykes (300–260 Ma, e.g., Aubele et al., 2014) that trend NE in NE Sardinia and Corsica and NNW in S Sardinia, south of the NE-trending Nuoro strike-slip fault system (Bigi et al., 1992; Figure 2a). Patches of lower Permian-lower Triassic silicic volcanic rocks and continental sedimentary rocks unconformably overlie the Paleozoic complex. The post-Hercynian history of Sardinia reflects the collapse of the orogen and the onset of Neo-Tethyan rifting in the Triassic similar to other southern European margins (e.g., Angrand et al., 2020). Shallow marine sedimentation of carbonatic rocks extended during mid-Triassic, Jurassic, and Cretaceous, covering the entire post-orogenic Sardinia. The Mesozoic sequence is now mainly exposed in ESE and NW Sardinia (Figure 2a), and records a period of relative tectonic quiescence, only interrupted in the mid-Cretaceous. The carbonate shelf sedimentation was halted by the sinistral strike-slip motion between the Iberian and European plates (Dewey et al., 1989; Handy et al., 2010; Le Breton et al., 2021; Stampfli & Borel, 2002; Wortmann et al., 2001). This tectonic phase, compatible with a N60° shortening direction (in present day-coordinates; Cherchi & Tremolieres, 1984) is recorded as low-angle angular unconformities. Bauxite pockets exposed along the unconformable contacts indicate a stratigraphic hiatus between the lower and upper Cretaceous strata (Mameli et al., 2007). Two low-temperature thermochronologic ages (fission tracks on apatites) of 99.3 ± 5.6 and 117.3 ± 6.5 Ma obtained at localities adjacent to the Nuoro fault system (Figure 2a) testify to local coeval exhumation of at least 3 km (Zattin et al., 2008).
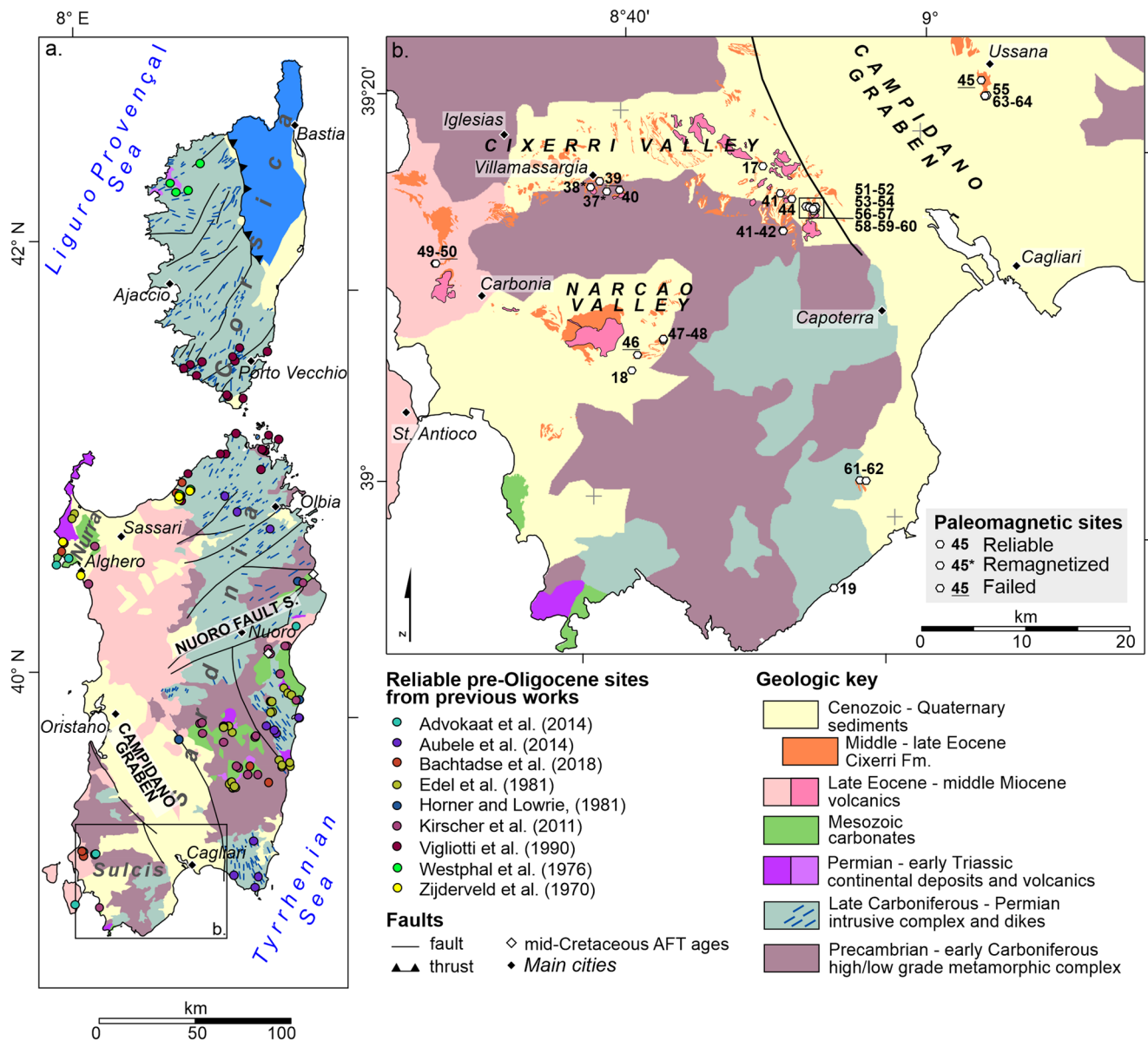
Figure 2. Geology of the Corsica-Sardinia microplate and paleomagnetic sampling sites. (a) Geologic map of Sardinia and Corsica Islands after Carmignani et al. (2016), together with reliable pre-Oligocene paleomagnetic sites from previous authors used in this study, and location of mid-Cretaceous apatite fission track data from Zattin et al. (2008). (b) Geologic map of Sulcis region after Carmignani et al. (2016) and 1:50,000 CARG maps for Cixerri Fm. outcrops location. Sampled paleomagnetic sites presented in this study are shown as white symbols.

Synchronous with the opening of the Bay of Biscay during Early to mid-Cretaceous times (e.g., Le Breton et al., 2021 and references therein), Iberia separated from Europe and rotated 35° CCW (Gong et al., 2008; Neres et al., 2012, 2013; Van der Voo, 1969). Two main tectonic scenarios (e.g., Barnett-Moore et al., 2016) can explain such event: (a) Iberia, along with Corsica-Sardinia, underwent a left-lateral motion up to 700 km with respect to Eurasia (Le Breton et al., 2021 and references therein), and a diffuse transtensional margin formed between Iberia and Europe (Asti et al., 2022; Jammes et al., 2009; Tugend et al., 2014); (b) as paleomagnetic data from Sardinia did not seem to record the 35° Iberian CCW rotation, Advokaat et al. (2014), Van der Voo (1969) and van Hinsbergen et al. (2020) advocated a scissor-like Iberia drift along the Bay of Biscay and contemporaneous shortening in the Pyrenees, separated by Corsica-Sardinia as a part of Provençal Europe by a ~N-S dextral transform fault.

Both geologic and paleontologic evidence (Chabrier & Mascle, 1975; Cherchi, 1979; Cherchi & Schroeder, 1976) suggests that the Corsica–Sardinia block was in continuity with the European–Iberian continental margin

during the Eocene. Subtle Pyrenaic deformation of latest Paleocene-early Eocene in age is reported in both SW Sardinia and N Sardinia-Corsica (e.g., Barca & Costamagna, 1997, 2010; Carmignani et al., 2004; Costamagna & Schäfer, 2018; Lacombe and Jolivet, 2005). The Pyrenaic shortening structures of SW Sardinia trend roughly N-S, thus they are assumed to have formed E-W—similarly to Pyrenees thrust faults—and subsequently to have been rotated CCW during the Oligo-Miocene Sardinia drift and rotation event. Pyrenaic deformation is also widespread in Provence, where it is represented by E-W folds and thrust fronts (Bestani et al., 2016; Lacombe and Jolivet, 2005; Séranne et al., 2021).

The Paleocene and Eocene Sardinian geologic record is represented by a marine to continental sedimentary sequence exposed in SW Sardinia (Sulcis; Figure 2b) unconformably overlying the Paleozoic basement and the Mesozoic carbonatic rocks. The sequence starts with Upper Paleocene continental sandstone and conglomerates (Barca & Costamagna, 2010). Lower Eocene marine carbonatic rocks (Miliolitico Fm.) are followed by a paralic sequence containing coal layers (Lignitifero Fm.), and a continental succession (Cixerri Fm.) bracketed in age between the early Lutetian (Lignitifero Fm. top layers ~45 Ma) and the beginning of the calk-alkaline magmatism of SW Sardinia, radiometrically dated here at 32 Ma (Beccaluva et al., 1985; Lustrino et al., 2009). Cenozoic volcanic rocks are interfingered with upper Oligocene-lower Miocene continental conglomerates (Ussana Fm.) evolving to lower-mid Miocene marine sedimentary rocks. Extensional tectonics related to the Liguro-Provençal basin spreading is documented in Sardinia not earlier than late Oligocene-early Miocene (24–22 Ma), whereas robust evidence both onshore and offshore the Gulf of Lion documents a late Oligocene (30 Ma) rifting onset and an early Miocene (21 Ma) breakup unconformity, indicating oceanic spreading (Séranne, 1999).

The Cixerri Fm. is exposed along the E-W oriented Cixerri and Narcao grabens (Sulcis), and few outcrops occur along the S Sardinia coast and on the eastern side of the Campidano Graben (Figure 2b; Barca & Costamagna, 1997, 2010; Carmignani et al., 2004; Costamagna & Schäfer, 2018). The exposures of W Sulcis are mostly characterized by alluvial gray sandstones and conglomerates, whereas reddish lacustrine silts and clays are exposed at both edges of the Campidano graben (Figure 3). Sedimentary features clearly show eastward paleo-flow directions in present-day coordinates (Barca & Costamagna, 2010; Costamagna & Schäfer, 2018). Mid-Cretaceous fossils from Cixerri pebbles indicated a Pyrenaic affinity (Cherchi, 1979), suggesting that the Cixerri Fm. is a molasse related to Pyrenees chain dismantling (Barca & Costamagna, 2010). The Cixerri Fm. strata are mostly undeformed (Barca & Costamagna, 1997) being sub-horizontal (Figure 3c and Table 1) and show primary sedimentary features typical of a continental fluvio-lacustrine environment, such as erosive channels (Figure 3a) and contacts (Figure 3b) with variable geometry and bedding attitudes (Figures 3d and 3h). The Cixerri Fm. shows very limited tectonic deformation as related to rare inverse faults observed in W Sulcis and associated to late Pyrenaic orogeny (Faccenna et al., 2002), and normal faults observed only nearby the Campidano graben and associated to the extensional tectonics characterizing W Sardinia since the late Oligocene (Figures 3e, 3f, and 3g).

3. Paleomagnetism of the Cixerri Fm.

3.1. Paleomagnetic Sampling and Methods

We collected a total of 289 paleomagnetic samples at 28 sites mainly from reddish lacustrine silts and clays levels of the mid-late Eocene age Cixerri Fm. (Figures 2b and 3). At each site, we drilled 8–12 cores (10 on average) using a petrol-powered portable drill cooled by water, and oriented them in situ using both a Sun and a magnetic compass, corrected for the local geomagnetic declination in April/September 2021 (~3°E according to NOAA's National Geophysical Data Center). Bedding attitude is mostly sub-horizontal reaching a maximum dip of 20–40° at six sites (Table 1). The 28 sampled sites were coupled with 3 Cixerri sites (26 samples) collected by Faccenna et al. (2002) for magnetic anisotropy measurements, for a total Cixerri data set of 31 sites (315 oriented cores).

The cores were cut into standard specimens of 22 mm height and paleomagnetic measurements were performed in the shielded room of the paleomagnetic laboratory at the Istituto Nazionale di Geofisica e Vulcanologia (Rome, Italy), using a 2G Enterprises direct current superconducting quantum interface device cryogenic magnetometer. All samples were thermally demagnetized using a Pyrox shielded oven in 10 steps up to 690°C. Assuming 600°–690°C as the temperature interval where primary magnetization from detrital hematite is isolated (Jiang et al., 2015), wide (50°C) temperature increments were used from 300°C to 600°C, and smaller (30°C) increments between 600°C and 690°C.
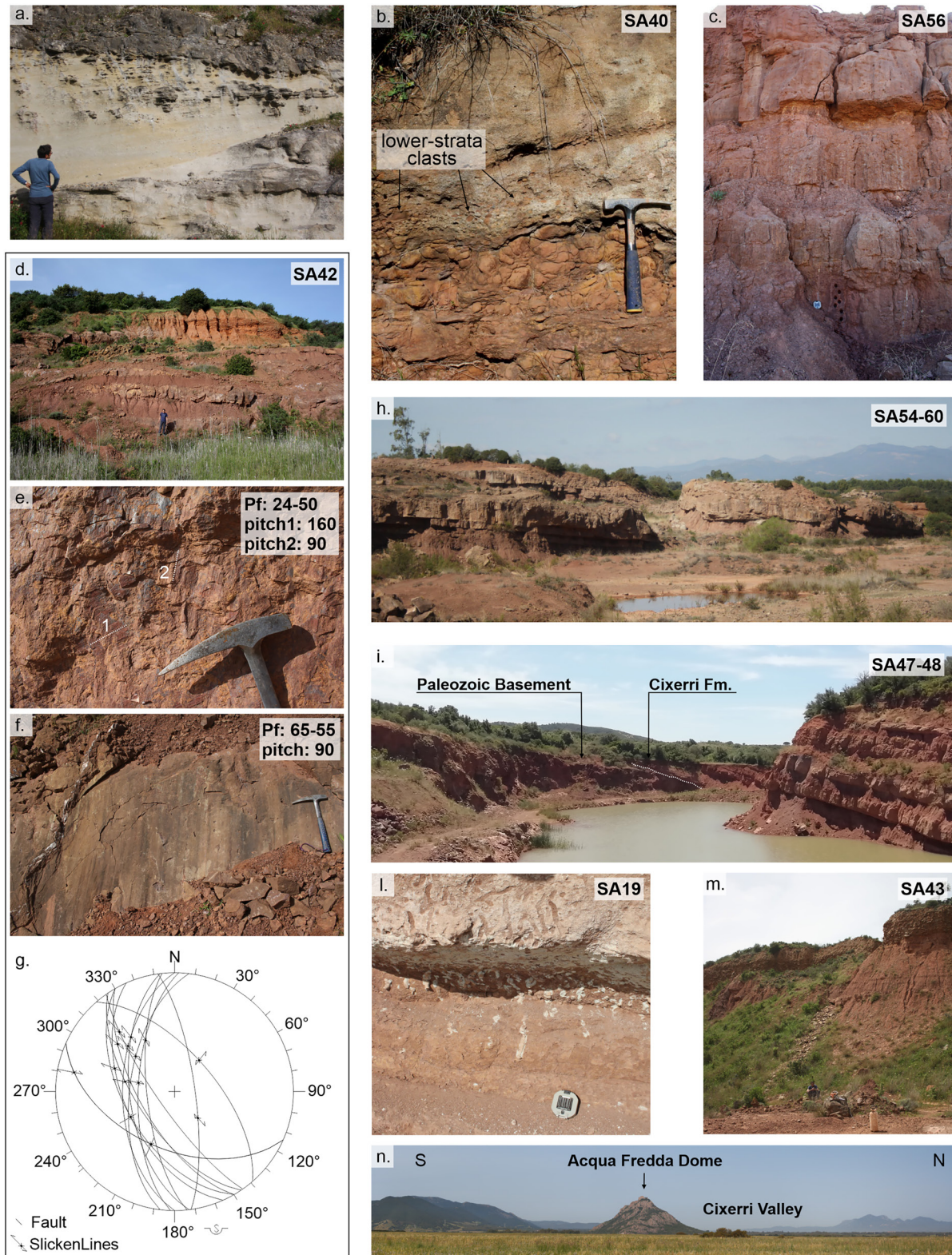
Figure 3.

Table 1
Paleomagnetic Directions From Mid-Upper Eocene Cixerri Fm. (SW Sardinia)

Sampled sites				Mean intensity (A/m * 10³)		In-situ characteristic remanent magnetization (ChRM)						Tilt-corrected ChRM	
Site	Latitude (°N)	Longitude (°E)	Bedding (dipdir-dip)	NRM	ChRM	n/N	State	D (°)	I (°)	k	α_{95} (°)	D (°)	I (°)
SA17[a]	39° 15.174′	8° 54.910′	SUB-HZT	18.32	5.73	5/8	N	279.5	39.8	45.9	11.4	279.5	39.8
SA18[a]	39° 7.290′	8° 42.118′	159–9	0.86	0.10	5/9	N	297.3	55.0	44.6	11.6	286.7	61.2
SA19[a]	38° 56.113′	8° 56.296′	65–5	5.40	2.55	9/9	N	301.9	39.4	120.4	4.7	305.6	42.0
SA37[b]	39° 15.803′	8° 39.469′	SUB-HZT	1.86	0.38	9/12	N	353.3	51.7	13.2	14.8	353.3	51.7
SA38[b]	39° 15.944′	8° 38.331′	20–13	44.99	14.73	10/10	N	341.6	72.8	16.6	12.2	357.3	61.5
SA39	39° 16.282′	8° 38.952′	95–10	-	-	-	-	-	-	-	-	-	-
SA40	39° 15.906′	8° 40.294′	40–5	3.13	0.22	10/10	N	308.0	43.4	10.7	15.5	312.8	43.4
SA41	39° 16.309′	8° 50.986′	43–24	1.01	0.48	10/10	R	91.5	−56.2	61.2	6.2	133.2	−65.4
SA42	39° 14.407′	8° 51.317′	280–10	1.36	0.30	11/11	R	101.5	−44.6	90.2	4.8	101.3	−34.6
SA43	39° 14.385′	8° 51.351′	275–3	1.63	0.25	12/12	R	78.2	−27.7	50.5	6.2	78.6	−24.9
SA44	39° 16.071′	8° 51.785′	42–30	5.83	1.82	7/11	R	83.2	−46.9	69.6	7.3	121.9	−62.8
SA45	39° 22.863′	9° 3.853′	36–13	-	-	-	-	-	-	-	-	-	-
SA46	39° 7.465′	8° 42.241′	SUB-HZT	-	-	-	-	-	-	-	-	-	-
SA47	39° 8.303′	8° 43.889′	266–17	3.37	0.83	10/10	N	255.3	67.2	37.9	7.9	259.5	50.4
SA48	39° 8.387′	8° 43.896′	304–22	4.77	0.62	10/10	N	274.8	63.8	309.0	2.8	286.7	43.5
SA49	39° 11.442′	8° 28.389′	215–27	0.51	0.23	10/11	R	94.9	−44.8	16.7	12.2	79.0	−27.8
SA50	39° 11.450′	8° 28.452′	225–46	-	-	-	-	-	-	-	-	-	-
SA51	39° 15.765′	8° 52.928′	163–5	0.84	0.50	10/10	R	104.5	−50.6	141.9	4.1	98.9	−52.9
SA52	39° 15.729′	8° 52.766′	351–19	1.89	0.97	10/10	R	73.0	−43.6	122.9	4.4	91.3	−43.2
SA53	39° 15.682′	8° 52.996′	SUB-HZT	2.46	1.31	10/10	R	114.9	−53.2	117.5	4.5	114.9	−53.2
SA54	39° 15.629′	8° 53.300′	279–11	0.56	0.24	10/10	R	101.4	−50.6	52.8	6.7	101.0	−39.6
SA55	39° 22.041′	9° 4.191′	SUB-HZT	0.39	0.13	9/10	R	121.5	−24.8	56.5	6.9	121.5	−24.8
SA56	39° 15.583′	8° 53.400′	SUB-HZT	0.44	0.17	7/11	R	108.5	−45.6	52.5	8.4	108.5	−45.6
SA57	39° 15.497′	8° 53.304′	339–15	11.91	5.31	10/10	R	60.4	−57.8	396.3	2.4	84.1	−56.9
SA58	39° 15.762′	8° 53.408′	SUB-HZT	0.48	0.19	9/10	R	98.1	−44.8	18.3	12.4	98.1	−44.8
SA59	39° 15.740′	8° 53.402′	SUB-HZT	0.48	0.21	8/10	R	104.1	−43.2	46.0	8.2	104.1	−43.2
SA60	39° 15.634′	8° 53.249′	141–17	0.82	0.25	8/9	R	108.3	−36.1	17.9	13.5	98.5	−49.7
SA61	39° 1.768′	8° 57.536′	342–11	0.73	0.39	9/10	R	85.1	−41.4	153.2	4.2	93.9	−38.1
SA62	39° 1.764′	8° 57.960′	356–10	2.25	0.48	10/10	N	288.8	46.8	39.5	7.8	297.4	41.7
SA63	39° 22.089′	9° 4.292′	79–31	1.17	0.13	7/11	R	109.3	−8.4	10.4	19.6	116.2	−34.4
SA64	39° 22.053′	9° 4.187′	SUB-HZT	0.43	0.13	4/11	N	291.1	38.1	24.8	18.8	291.1	38.1

Note. Site-mean intensity of the total natural remanent magnetization (NRM) and of the isolated characteristic remanent magnetization component (ChRM). n/N: number of samples giving reliable results/number of studied samples at a site. State N and R indicate normal- and reverse-polarity magnetization, respectively. D and I: site-mean declination and inclination calculated before and after tilt correction; k and α_{95}: statistical parameters after Fisher (1953).
[a]Paleomagnetic sites from Faccenna et al. (2002). [b]Discarded sites due to magnetic overprint.

Figure 3. Field observations from the Cixerri Fm. highlight a fluvial-alluvial to lacustrine sedimentary environment. (a) Coarse sand erosive fluvial channel in western Sulcis. (b) Erosive high-energy environment contact between layers of the Cixerri Fm. at sampling site SA40. (c) Alternating horizontal lacustrine silty clay and fine sand layers at site SA56. (d) Panoramic view of ~10 m thick Cixerri outcrop at sites SA42. Notice the varying geometry of clay and sand layers as related to the fluvial-alluvial depositional environment. (e, f, and g) Extensional deformation at sites SA42 likely reflect the Campidano Graben Plio-Pleistocene deformation. (h) Thick sandy layers eroding the underling silty clay layers in a vast quarry at sites SA54 and SA60. (i) Sedimentary contact of the Cixerri Fm. over the Hercynian basement at sites SA47–48. (l) Fossil worm's traces formed in soft sediments at site SA19. (m) ~15 m thick outcrop of fine-grained lacustrine layers at site SA43. (n) Panoramic view of the Cixerri Valley looking to the West and the Late Oligocene Acqua Fredda volcanic Dome.

Demagnetization data were plotted on orthogonal vector diagrams (Zijderveld, 1967), and principal component analysis was performed to isolate magnetization components (Kirschvink, 1980). Site-mean paleomagnetic directions were computed using Fisher's (1953) statistics and plotted on equal-area projections, using the Remasoft software (Chadima & Hrouda, 2006). Paleomagnetic rotation and flattening values with respect to Europe were calculated according to Demarest (1983), using reference paleo-poles from Torsvik et al. (2012).

Finally, the magnetic mineralogy was investigated for one representative specimen per site by thermal demagnetization of a three-component isothermal remanent magnetization (IRM) according to Lowrie (1990). A magnetic field of 2.7, 0.6, and 0.12 T was imparted along the three sample axes with a 2G Enterprises pulse magnetizer. Samples were subsequently thermally demagnetized in 10 steps up to 680°C.

3.2. Results

Scattered or erratic (uninterpretable) demagnetization diagrams were observed at four sites that were excluded from further considerations (Table 1). In the remaining 27 sites, a viscous component was unblocked by 300°C (Figure 4). In 96% of the samples a dual polarity characteristic remanent magnetization (ChRM) was identified in the 300–540/690°C interval. At site SA41 nearly antipodal high temperature (HT; 610–690°C) and low temperature (LT; 300–610°C) components were identified (Figure 4), and the site-mean direction was calculated by LTs as the HTs are of low intensity and often scattered.

The α_{95} values associated with estimated site-mean paleomagnetic directions range from 2.4 to 19.6°, 9.0° on average (Table 1). The values of the Fisher (1953) k and α_{95} statistical parameters do not vary from in-situ to tilt-corrected coordinates, as bedding attitude is mostly constant within a site. At sites SA56 and SA61—showing variable bedding—the k and α_{95} decrease and increase insignificantly, respectively. Ten (seventeen) sites yield a normal (reverse) polarity magnetization (Figure 5). Directions from sites SA37 and SA38 are undistinguishable from the geocentric axial dipole (GAD) local field direction, and were therefore considered as recently remagnetized and excluded from further consideration. A mean direction calculated for the remaining 25 sites yield an in-situ $D = 281.0°$, $I = +45.7°$; $k = 23.7$, $\alpha_{95} = 6.1°$ and tilt-corrected $D = 283.9°$, $I = +45.1°$; $k = 27.5$, $\alpha_{95} = 5.6°$.

The McFadden and McElhinny (1990) reversal tests performed on both in-situ and tilt-corrected directions is positive of type C (Table S1 in Supporting Information S1). Due to the prevailing sub-horizontal bedding attitudes at the sampling sites, the fold test could not be applied. Additionally, considering widespread evidence of a fluvial-alluvial depositional environment for the Cixerri Fm. (Figure 3; Barca & Costamagna, 2010; Costamagna & Schäfer, 2018), we suggest that the measured bedding attitudes reflect original sedimentary features, rather than tectonic tilting. The virtually undeformed Cixerri Fm. deposited as a distal molasse of the Pyrenees and the unique significant faulting recognized in the field is likely related to Plio-Pleistocene Campidano Graben extension, that however did not yield significant bed tilting (Figures 3e, 3f, and 3g).

The thermal demagnetization of a three-axis IRM shows that the high (≥ 2.7 T) and intermediate coercivity ($0.12 <$ coercivity ≤ 0.6 T) fractions dominate remanence in 23 sites and are unblocked at 670–690°C showing mostly a convex behavior (Figures S1a and S1b in Supporting Information S1) typical for detrital hematite (Jiang et al., 2015). At half of the sites, the hard fraction shows also a significant drop at 120°C. The soft coercivity fraction (≤ 0.12 T) is virtually absent except at site SA38, where is demagnetized at 600°C. Such data suggest that the main magnetic carrier of the Cixerri Fm. is detrital hematite, coupled with goethite at about half of the sites and magnetite at site SA38.

The antipodality of the principal magnetization components recovered in the Cixerri dataset indicates a primary magnetization where the main mineralogic magnetic carrier is detrital hematite and subordinate goethite. The observed bedding in fluvial-alluvial beds is most likely an original depositional feature, implying that unfolding would yield biased paleomagnetic directions.

Magnetic overprints at sites SA37 and 38 may be related to both local lithologic and magnetic mineralogy characteristics, as site SA37 was sampled in coarse-grained sandy layers (Figure S2 in Supporting Information S1), whereas SA38 is the only site containing magnetite, in contrast to the predominant hematite and goethite content observed in the other sites.
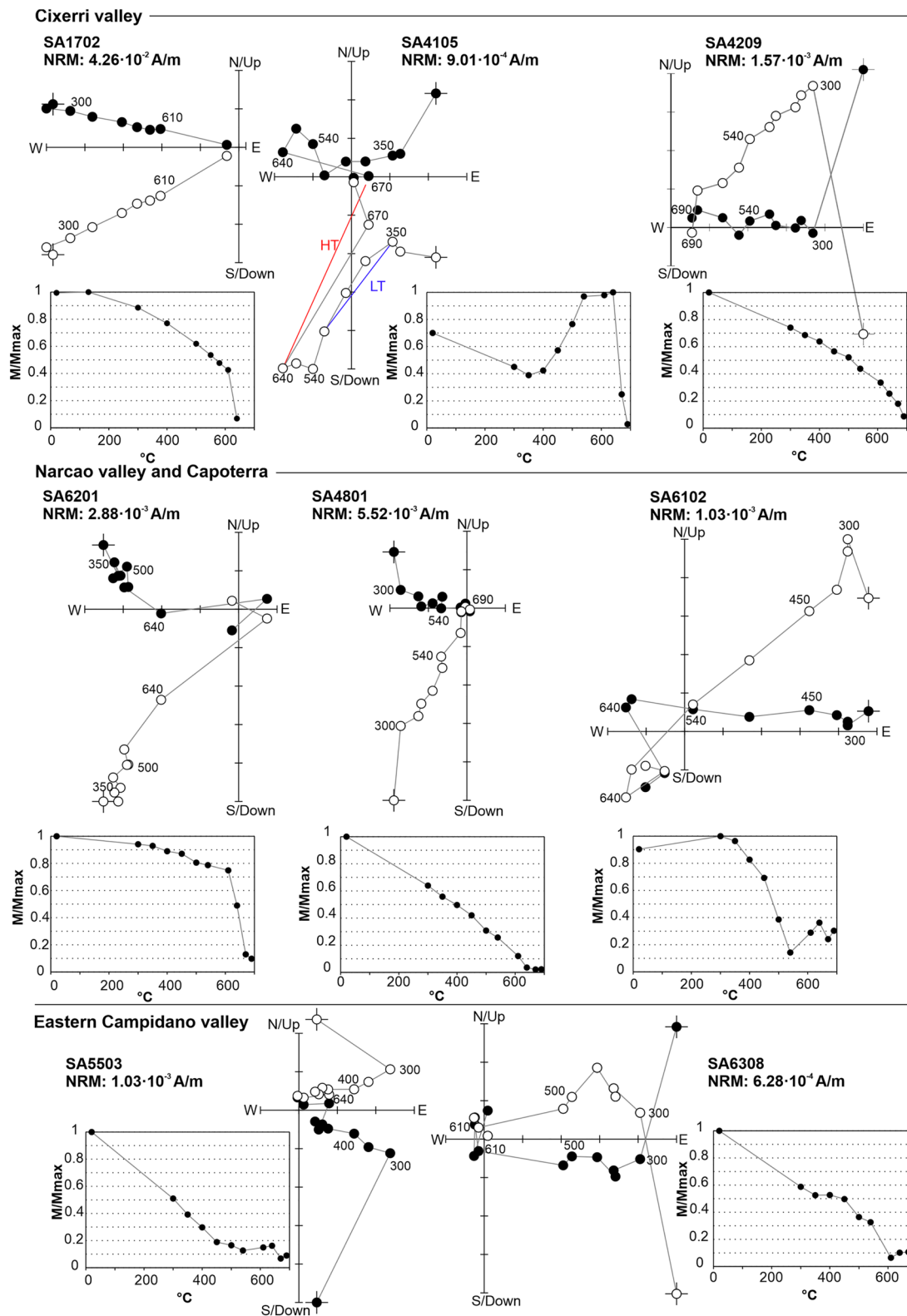
Figure 4. Orthogonal vector diagrams of typical demagnetization data, in-situ coordinates. Solid and open circles represent projection on the horizontal and vertical planes, respectively. Demagnetization steps are in °C. Normalized intensity of magnetization versus temperature graphs are also reported.
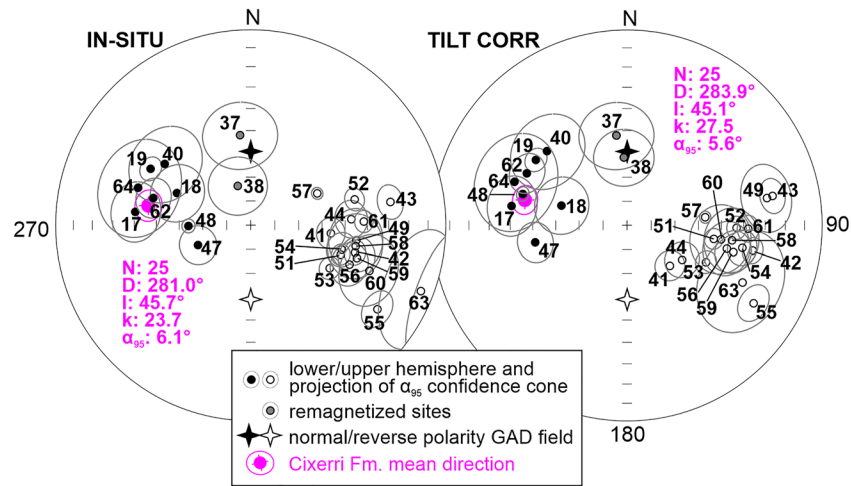
Figure 5. Equal area projection of the site-mean paleomagnetic directions from the Cixerri Fm.

4. Permian-Eocene Paleomagnetic Directions and Rotations

When considered in the normal polarity state, the 25 in-situ directions from the Cixerri Fm. yield a mid-late Eocene age paleomagnetic direction for SW Sardinia defined by: $D = 281.0°$, $I = +45.7°$ and $\alpha_{95} = 6.1°$. The rotation (R) and flattening (F) values calculated with respect to Europe for a 40 Ma paleopole (Torsvik et al., 2012) are $R = 86.4 \pm 7.3°$ CCW and $F = 6.8 \pm 5.3°$.

This result was compared to previously published data from both Sardinia and Corsica (Table 2). The Miocene rotation path of the whole Corsica-Sardinia block was taken from mean values reported by Gattacceca et al. (2007) and Speranza et al. (2002). Considering paleomagnetic data similarity in early Miocene times, we averaged out directions from S Sardinia, and N Sardinia-Corsica (their tectonic boundary being the Nuoro fault) and superimposed them over European expected declinations (Figure 6). Pre-Miocene paleomagnetic data were re-analyzed considering stringent statistical criteria, that is, hierarchically averaging out independent site-mean directions

Table 2
Re-Evaluated Mean Paleomagnetic Directions From Corsica and Sardinia, and Rotation-Flattening Values With Respect to Europe

ID	Location	Lithology	Age	Age range (Ma)	N	D (°)	I (°)	k	α_{95} (°)	R (°)	ΔR (°)	F (°)	ΔF (°)
A	Corsica	Dikes	Lower-mid Permian	286–264	15	322.8	7.2	15.3	10.1	−57.9	8.2	5.4	9.0
B	North Sardinia	Dikes	Lower-mid Permian	286–264	14	312.8	1.5	47.2	5.8	−67.9	5.0	11.0	6.2
C	North Sardinia	Volcanics/sediments	Lower-mid Permian	298.8–266.5	16	314.8	8.9	17.8	9.0	−65.4	7.4	−8.1	8.3
D	South Sardinia	Dikes	Lower-mid Permian	303–285	10	267.4	11.1	17.9	12.0	−113.2	12.5	−17.5	12.9
E	South Sardinia	Volcanics/sediments	Lower-mid Permian	302–291.7	8	259.6	4.1	32.4	9.9	−121.7	10.3	−6.6	11.3
F	South Sardinia	Carbonates	Mid Jurassic	179–158	14	266.8	45.1	23.9	8.3	−112.9	10.0	−3.2	8.0
G	South Sardinia	Carbonates	Upper Jurassic	161–147	7	283.8	48.8	37.6	10.0	−86.9	13.1	−5.6	10.1
H	South Sardinia	Carbonates	Lower Eocene	57–47	4	263.9	38.4	52.8	12.8	−101.3	13.0	10.0	10.3
I (CIX)	South Sardinia	Red beds	Mid-Upper Eocene	45–32	25	281.0	45.7	23.6	6.1	−86.4	7.3	6.8	5.3
L	Sardinia	Volcanics	Burdigalian	21–20	35	320.6	46.4	15.0	6.4	−43.4	7.6	7.7	5.4
M	Sardinia	Marine clays	Aquitanian/Burdigalian	19.2–18.9	24*	340.6	39.3	58.6	3.9	−23.4	4.6	14.8	3.7
N	Sardinia	Volcanics	Burdigalian/Langhian	15.8–15.1	9	357.9	43	11.0	12.3	−6.1	13.4	11.0	9.8

Note. All mean directions are considered in normal polarity. N: number of sites used to calculate the mean paleomagnetic directions (*number of specimens from a section, Speranza et al., 2002): Declination (D) and Inclination (I); k and α_{95}: statistical parameters after Fisher (1953). Miocene directions relative to the whole Sardinia block are from Gattacceca et al. (2007) and Speranza et al. (2002). Rotation (R) and flattening (F) values, and relative errors ΔR and ΔF (according to Demarest (1983)) are evaluated with respect to Europe using paleopole directions from Torsvik et al. (2012).
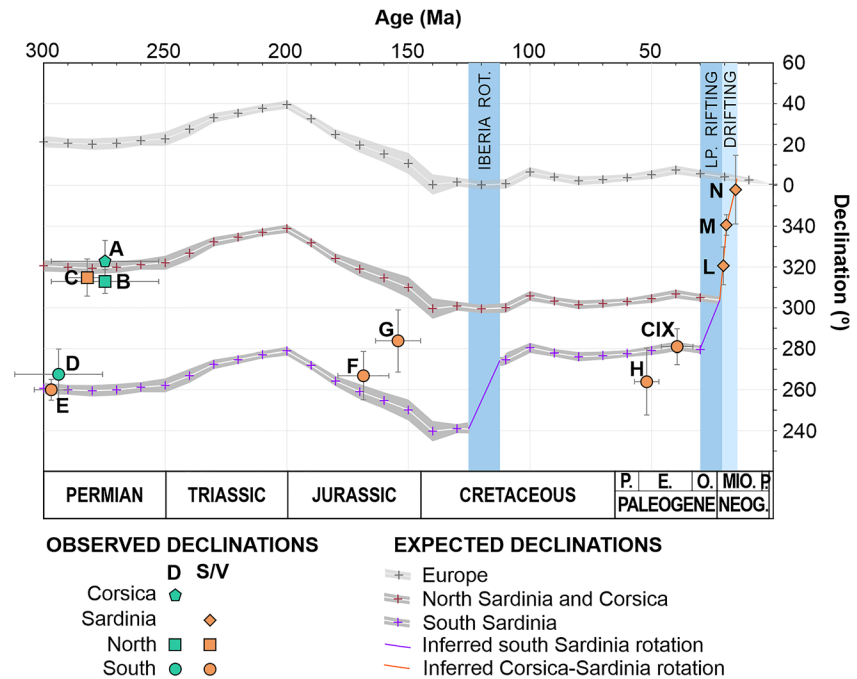
Figure 6. Paleomagnetic declinations versus age from Sardinia and Corsica sites, superimposed on expected European declinations, rotated counterclockwise by 60, 86, and 120°, at central Sardinia coordinates (see text). Occurrence timing of Iberia rotation (ROT.) and Liguro-Provençal (LP.) rifting-drifting are reported in light blue shades. Data ID as listed in Table 2. D, dikes; S/V, sediments and volcanics.

of similar age to get well-constrained ($k > 10$ and $\alpha_{95} < 15°$) regional paleomagnetic directions. We excluded site-mean directions characterized by: (a) less than 3 samples per site; (b) $k < 10$; (c) likely remagnetized sites yielding in situ paleomagnetic directions similar to the local GAD field direction at mid Sardinian coordinates ($D = 0°$; $I = 59°$).

Permian volcanic rocks, sedimentary rocks, and dykes (Aubele et al., 2014; Bachtadse et al., 2018; Edel et al., 1981; Zijderveld et al., 1970) provide coherent shallow inclination directions of the same polarity that are fully consistent with coeval equatorial position of south Europe as a part of Pangea (Torsvik et al., 2012). This evidence strengthens the reliability of available radiometric ages from Permian rocks, as older (younger) ages would imply southern (northern) hemisphere location, and excludes the occurrence of younger magnetic overprints. We systematically assume a reverse polarity of the Permian rocks as: being consistent with the Kiaman long reverse polarity chron (310–260 Ma); and reverse polarity Permian data from N Sardinia and Corsica yield a 50–60° CCW rotation with respect to Europe that is consistent with the Miocene age rotation (Figure 6).

Considering S Sardinia, pre-40 Ma age European declinations rotated CCW by ~86° (our rotation value from the Cixerri Fm.) are consistent with early Eocene data by Advokaat et al. (2014). European directions are definitely not consistent with Permian data from S Sardinia if only a ~90° CCW rotation is considered, but they coincide when the 35° CCW rotation of Iberia is added (Gong et al., 2008; Van der Voo, 1969). Although the timing of Iberia rotation is still controversial within an Early-mid Cretaceous (120–150 Ma) time window (Neres et al., 2012, 2013) we assume the mid-Cretaceous age (Aptian) proposed by Gong et al. (2008). The resulting ~120° CCW rotated European declinations are also consistent with Middle Jurassic data from southern Sardinia, whereas Late Jurassic age declinations are significantly smaller. We suggest that the Late Jurassic data (data point G in Figure 6) are biased by remagnetization, as all Mesozoic carbonatic rocks are weakly magnetized with magnetite and goethite as remanence carriers, and generally yield highly scattered results as well as frequent evidence for magnetization overprint (Advokaat et al., 2014; Horner & Lowrie, 1981; Kirscher et al., 2011). Furthermore, when considered together, the Middle and Late Jurassic age data (data points F and G in Figure 6) yield an apparent CCW rotational trend, whereas Europe rotated CW by about 40° during the entire Jurassic (Figure 6).
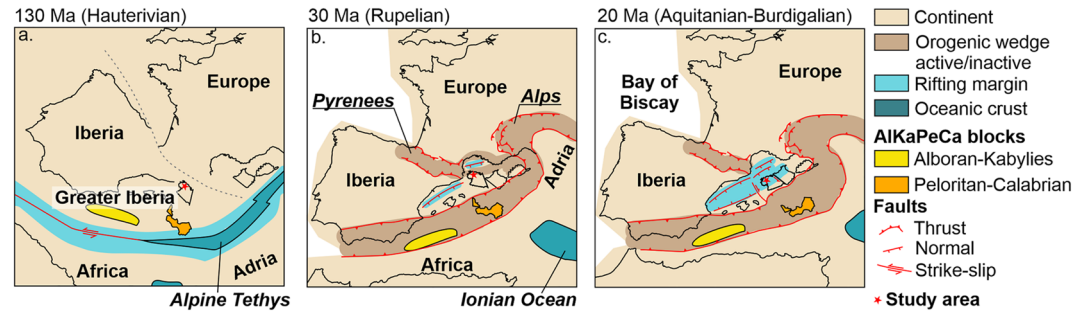
Figure 7. Evolutionary paleogeographic model of the western-central Mediterranean domain. Gray dashed line in panel (a) indicate the future (Aptian) Iberia-Europe boundary.

The outlined scenario would require a ~65° declination difference between Triassic-Jurassic data from southern and northern Sardinia. Unfortunately, this is impossible to verify due to the lack of Mesozoic results from NW Sardinia that pass our statistical criteria (Table S2 in Supporting Information S1). Only two and none of the Jurassic sites from Nurra by Kirscher et al. (2011) and Advokaat et al. (2014), respectively, pass our statistic criteria, so that the Jurassic Sardinia paleomagnetism of rocks north of the Nuoro fault is virtually unconstrained. The Triassic dolomites from Nurra (one site, Advokaat et al., 2014) and S Sardinia (three sites, Horner & Lowrie, 1981) were likely remagnetized during the Meso-Cenozoic as (a) their paleo-inclination is steeper than coeval expected European inclinations (e.g., Advokaat et al., 2014), (b) all sites show a normal polarity, and (c) the three directions by Horner and Lowrie (1981) show very clustered directions ($k = 1,245$) that do not average out the paleo-secular variation of the geomagnetic field. Middle-Late Jurassic paleomagnetic data from a magnetostratigraphic study of the Mt. Albo succession by Muttoni et al. (2018) were excluded as the sampling area is located within the deformation zone of the Nuoro fault system and cannot be used to infer the vertical axis rotation of an entire microplate.

5. Evolution of an Iberian-Affinity S Sardinia Block and Late Oligocene Assembly of the Corsica-Sardinia Microplate

We suggest that S Sardinia was part of Iberia and located just SE of the Pyrenees before early Oligocene (30 Ma) rifting in the Liguro-Provençal realm (Figure 7). S Sardinia fits well in a clear reentrant of the 2,500 m bsl isobath NE of the Balearic Islands (Figure 1). We suggest that it first rotated 35° CCW along with Iberia during the Aptian,—whereas N Sardinia-Corsica lay adjacent to Provence—then underwent a further ~30° rotation during Oligocene-early Miocene Liguro-Provençal Basin rifting.

The Nuoro fault separates the two Sardinian blocks, is a complex crustal structure cutting both Hercynian and mid-Late Jurassic rocks, and fading out westward below Miocene volcanics and sediments (Figure 2a), although Oligo-Miocene volcanic rocks in central Sardinia are locally cut by recent fault re-activation. The late Oligocene-early Miocene left-lateral strike-slip fault activity of the Nuoro fault is firmly constrained by syntectonic Aquitanian sedimentary rocks (Bigi et al., 1992; Carmignani et al., 2004). An older mid Cretaceous activity is obviously difficult to assess lacking coeval sedimentary rocks around the fault. However, widespread transpressive deformation of mid-Cretaceous age is documented as related to Iberia—Europe convergence (Dewey et al., 1989; Handy et al., 2010; Le Breton et al., 2021; Stampfli & Borel, 2002; Wortmann et al., 2001).

Mid-Cretaceous limestones from NW Sardinia are interrupted by a clear discontinuity and hiatus hosting bauxite pockets that is stratigraphically constrained between lower Aptian and Cenomanian strata (Bigi et al., 1992; Filigheddu & Oggiano, 1984; Philip & Allemann, 1982). Here, as well as in the Pyrenees-Provençal domain, surface exposure of the shelf carbonates under favorable climatic conditions resulted in lateritic weathering (Mameli et al., 2007). Such emergence has been related to transpressional deformation that resulted in uplifted blocks and wide antiform and synform structures (Combes, 1990; Combes et al., 1993; Oggiano et al., 1987). A N60° shortening direction (in present-day coordinates) has been reconstructed for this tectonic phase (Cherchi & Tremolieres, 1984). Apatite fission track data from rocks ~10 km to the south of the Nuoro fault indicate that rock exhumation was coeval with the mid-Cretaceous discontinuity (Zattin et al., 2008), likely related to fault block exhumation in a transpressive tectonic setting (e.g., Siravo et al., 2020; Xypolias et al., 2003; Mazzoli & Algarra, 2011).

The Pyrenaic affinity of the Cixerri Fm. was suggested by Cherchi (1979), who described pebbles from conglomeratic layers containing mid-Cretaceous fossils. Such fauna assemblage is notably absent from Sardinian carbonatic rocks but it is present in the southern Pyrenees. Conglomerates coeval with the Cixerri Fm. containing similar fossils also occur in the Balearic Islands, whereas the Cixerri Fm. totally lacks clasts from local Cambrian limestones that are widespread in W Sulcis. We conclude, in agreement with Barca and Costamagna (2010), that the Cixerri Fm. represent a late orogenic molasse located SE of the Pyrenees that received debris from chain dismantling. Compressive N-S structures documented in SW Sulcis (Barca & Costamagna, 2010; Carmignani et al., 2004) are consistent with NNW magnetic lineations documented by Faccenna et al. (2002), and suggest that the Cixerri Fm. was locally affected by the last late Eocene-early Oligocene Pyrenaic compressive episodes. When back-rotated by 90° according to our paleomagnetic data, the compressive structures have ∼E-W trends that are effectively sub-parallel to the Pyrenees (Figure 7).

After the 30° CCW rotation of S Sardinia during the 30–21 Ma Liguro-Provençal rifting episode well documented in the Gulf of Lion (Séranne, 1999), oceanic breakup occurred, and the Corsica-Sardinia block rotated as a whole ∼60° CCW in the 21–15 Ma time window along with oceanic crust emplacement in the Liguro-Provençal Sea. A 60° CCW rotation of Corsica-Sardinia after 21 Ma is consistent with data by Gattacceca et al. (2007).

Our rotation scenario reconciles CCW rotations documented in Permian and Miocene rocks from N Sardinia-Corsica, and explains the large magnitude CCW rotation based on data from Permian dykes and volcanic rocks from S Sardinia considering the sum of mid-Cretaceous and late Oligocene-early Miocene rotations of a S Sardinia block. The 65° excess CCW rotation of S Sardinia perfectly explains the 60° angle observed between trends of early Permian dykes in S Sardinia and N Sardinia-Corsica (Figure 2a).

As Calabria was likely located adjacent to Sardinia prior to 10–2 Ma Tyrrhenian Sea spreading (Kastens et al., 1988; Mattei et al., 2002; Nicolosi et al., 2006), the 120° post-Jurassic CCW rotation documented in S Sardinia should, in principle, also be recorded on the Calabrian block. The almost ubiquitous occurrence of igneous-metamorphic rocks has always hampered paleomagnetic investigations on the Calabrian terrane, until Siravo et al. (2022) reported the first robust paleomagnetic results from Jurassic Ammonitico Rosso limestones locally lying over the Sila Massif in NE Calabria. The data are consistent with preliminary results by Manzoni (1979) and Manzoni and Vigliotti (1983) and document a 160° CCW Calabria rotation occurring between the Early Cretaceous and the mid-Miocene. Siravo et al. (2022) suggested that of these, about 90° occurred along with Sardinia during Eocene-Miocene (considering data and rotation timing by Advokaat et al., 2014), whereas the remaining 70° were due to Early-mid Cretaceous left-lateral transcurrent motion between Africa and Europe. Our new results and data compilation may conversely suggest that 120° of the 160° Calabria rotation occurred along with S Sardinia during 35° Aptian Iberia rotation and 90° Oligo-Miocene rotation related to Liguro-Provençal Basin rift-drift episodes (Figure 7).

Our proposed reconstruction would imply that Iberia, S. Sardinia, Balearic Islands and Calabria, along with adjacent Peloritan, Kabylies and Alboran internal terrains (Alvarez et al., 1974), formed a unique crust block that we call "Greater Iberia" before the early Oligocene (30 Ma) Liguro-Provençal onset of rifting (Figure 7), and that Early Cretaceous CCW rotation of Calabria related to transcurrent Alpine Tethyan tectonics was limited to a more realistic ∼40° magnitude. Greater Iberia margin consumption started during early Cenozoic at 50–40 Ma, considering average high-pressure peak metamorphism age estimate observed in the AlKaPeCa blocks that testify their incorporation into the proto-Alpine wedge (e.g., Amodio-Morelli et al., 1976; Angrand & Mouthereau, 2021; Rossetti et al., 2004 and references therein). Afterward, the Greater Iberia fragmentation and definitive separation from Iberia itself occurred at ∼30 Ma, during the onset of Liguro-Provencal rifting. We consider the traditionally assumed semi-rigid Iberia plate during the Mesozoic, differently than a recent reconstruction hypothesizing the occurrence of multiple Iberian micro plates eventually assembled in mid Cretaceous times (King et al., 2023).

We think that our proposed geodynamic model best fits existing paleomagnetic and tectonic evidence from Iberia, Corsica, and Sardinia. Further amendments await new paleomagnetic evidence, hopefully solving the two less solid points of our reconstruction: the unequivocal definition of Iberia rotation (at present bracketed in the 120–150 Ma time window), and the quantification of the possible differential rotations between S and N Sardinia by additional data of high quality between Permian and Miocene time.

Data Availability Statement

References

Advokaat, E. L., van Hinsbergen, D. J., Maffione, M., Langereis, C. G., Vissers, R. L., Cherchi, A., et al. (2014). Eocene rotation of Sardinia, and the paleogeography of the western Mediterranean region. *Earth and Planetary Science Letters*, *401*, 183–195. https://doi.org/10.1016/j.epsl.2014.06.012

Alvarez, W., Cocozza, T., & Wezel, F. C. (1974). Fragmentation of the Alpine orogenic belt by microplate dispersal. *Nature*, *248*(5446), 309–314. https://doi.org/10.1038/248309a0

Amodio-Morelli, L., Bonardi, G., Colonna, V., Dietrich, D., Giunta, G., Ippolito, F., et al. (1976). L'arco Calabro-Peloritano nell'orogene appenninico-maghrebide. *Memorie della Società Geologica Italiana*, *17*, 1–60.

Angrand, P., & Mouthereau, F. (2021). Evolution of the Alpine orogenic belts in the Western Mediterranean region as resolved by the kinematics of the Europe-Africa diffuse plate boundary. *BSGF-Earth Sciences Bulletin*, *192*(1), 42. https://doi.org/10.1051/bsgf/2021031

Angrand, P., Mouthereau, F., Masini, E., & Asti, R. (2020). A reconstruction of Iberia accounting for Western Tethys–North Atlantic kinematics since the late-Permian–Triassic. *Solid Earth*, *11*(4), 1313–1332. https://doi.org/10.5194/se-11-1313-2020

Asti, R., Saspiturry, N., & Angrand, P. (2022). The Mesozoic Iberia-Eurasia diffuse plate boundary: A wide domain of distributed transtensional deformation progressively focusing along the North Pyrenean Zone. *Earth-Science Reviews*, *230*, 104040. https://doi.org/10.1016/j.earscirev.2022.104040

Aubele, K., Bachtadse, V., Muttoni, G., & Ronchi, A. (2014). Paleomagnetic data from Late Paleozoic dykes of Sardinia: Evidence for block rotations and implications for the intra-Pangea megashear system. *Geochemistry, Geophysics, Geosystems*, *15*(5), 1684–1697. https://doi.org/10.1002/2014gc005325

Bachtadse, V., Aubele, K., Muttoni, G., Ronchi, A., Kirscher, U., & Kent, D. V. (2018). New early Permian paleopoles from Sardinia confirm intra-Pangea mobility. *Tectonophysics*, *749*, 21–34. https://doi.org/10.1016/j.tecto.2018.10.012

Barca, S., & Costamagna, L. G. (1997). Compressive "Alpine" tectonics in western Sardinia (Italy): Geodynamic consequences. *Comptes Rendus de l'Académie des Sciences-Series IIA-Earth and Planetary Science*, *325*(10), 791–797. https://doi.org/10.1016/s1251-8050(97)82758-9

Barca, S., & Costamagna, L. G. (2010). New stratigraphic and sedimentological investigations on the Middle Eocene–Early Miocene continental successions in southwestern Sardinia (Italy): Paleogeographic and geodynamic implications. *Comptes Rendus Geoscience*, *342*(2), 116–125. https://doi.org/10.1016/j.crte.2010.01.009

Barnett-Moore, N., Hosseinpour, M., & Maus, S. (2016). Assessing discrepancies between previous plate kinematic models of Mesozoic Iberia and their constraints. *Tectonics*, *35*(8), 1843–1862. https://doi.org/10.1002/2015tc004019

Beccaluva, L., Civetta, L., Macciotta, G., & Ricci, C. A. (1985). Geochronology in Sardinia: Results and problems. *Rendiconti della Società Italiana di Mineralogia e Petrologia*, *40*(5), 57–72.

Bestani, L., Espurt, N., Lamarche, J., Bellier, O., & Hollender, F. (2016). Reconstruction of the Provence Chain evolution, southeastern France. *Tectonics*, *35*(6), 1506–1525. https://doi.org/10.1002/2016tc004115

Bigi, G., Coli, M., Cosentino, D., Dal Piaz, G. V., Parotto, M., Sartori, R., & Scandone, P. (1992). *Structural model of Italy scale 1:500.000, sheet 3. C.N.R., Progetto Finalizzato Geodinamica*. SELCA Firenze.

Carmignani, L., Funedda, A., Oggiano, G., & Pasci, S. (2004). Tectono-sedimentary evolution of southwest Sardinia in the Paleogene: Pyrenaic or Apenninic dynamic? *Geodinamica Acta*, *17*(4), 275–287. https://doi.org/10.3166/ga.17.275-287

Carmignani, L., Oggiano, G., Funedda, A., Conti, P., & Pasci, S. (2016). The geological map of Sardinia (Italy) at 1: 250,000 scale. *Journal of Maps*, *12*(5), 826–835. https://doi.org/10.1080/17445647.2015.1084544

Chabrier, G., & Mascle, G. (1975). Comparaison des evolution geologiques de la Provence et de la Sardaigne (A partir d'exemples de la region Toulonnaise et de la Nurra Sarde). *Revue de Géographie Physique et de Géologie Dynamique*, *17*(2), 121–136.

Chadima, M., & Hrouda, F. (2006). Remasoft 3.0 a user-friendly paleomagnetic data browser and analyzer. *Travaux Géophysiques*, *27*, 20–21.

Cherchi, A. (1979). Microfaune aptiano-albiane dei ciottoli urgoniani della "Formazione del Cixerri" (Sardegna SW) e loro interesse paleogeografico. *Rivista Italiana di Paleontologia*, *85*(2), 353–410.

Cherchi, A., & Schroeder, R. (1976). Presence de galets du Vraconien superieur-Cenomanien basal de provenance iberique dans le Paleogene continental du Sud-Ouest de la Sardaigne. *Bulletin de la Société Géologique de France*, *18*(5), 1217–1219. https://doi.org/10.2113/gssgfbull.s7-xviii.5.1217

Cherchi, A., & Tremolieres, P. (1984). Nouvelles données sur l'évolution structurale au Mésozoïque et au Cénozoïque de la Sardaigne et leurs implications géodynamiques dans le cadre méditerranéen. *Comptes-Rendus des Séances de l'Académie des Sciences. Série 2, Mécanique-Physique, Chimie, Sciences de l'Univers, Sciences de la Terre*, *298*(20), 889–894.

Combes, P. J. (1990). Typologie, cadre géodynamique et genèse des bauxites françaises. *Geodinamica Acta*, *4*(2), 91–109. https://doi.org/10.1080/09853111.1990.11105202

Combes, P. J., Oggiano, G., & Temussi, I. (1993). Geodynamique des bauxites sardes, typologie, génese et controle paleotectonique. *Comptes Rendus de l'Académie des Sciences. Série 2, Mécanique, Physique, Chimie, Sciences de l'Univers, Sciences de la Terre*, *316*(3), 403–409.

Costamagna, L. G., & Schäfer, A. (2018). Evolution of a Pyrenean molassic basin in the Western Mediterranean area: The Eocene–Oligocene Cixerri formation in Southern Sardinia (Italy). *Geological Journal*, *53*(1), 424–437. https://doi.org/10.1002/gj.2911

De Jong, K. A., Manzoni, M., & Zijderveld, J. D. A. (1969). Palaeomagnetism of the Alghero trachyandesites. *Nature*, *224*(5214), 67–69. https://doi.org/10.1038/224067a0

Demarest, H. H., Jr. (1983). Error analysis for the determination of tectonic rotation from paleomagnetic data. *Journal of Geophysical Research*, *88*(B5), 4321–4328. https://doi.org/10.1029/jb088ib05p04321

Dewey, J. F., Helman, M. L., Knott, S. D., Turco, E., & Hutton, D. H. W. (1989). Kinematics of the western Mediterranean. *Geological Society, London, Special Publications*, *45*(1), 265–283. https://doi.org/10.1144/gsl.sp.1989.045.01.15

Edel, J. B., Montigny, R., & Thuizat, R. (1981). Late Paleozoic rotations of Corsica and Sardinia: New evidence from paleomagnetic and K-Ar studies. *Tectonophysics*, *79*(3–4), 201–223. https://doi.org/10.1016/0040-1951(81)90113-x

Faccenna, C., Becker, T. W., Lucente, F. P., Jolivet, L., & Rossetti, F. (2001). History of subduction and back arc extension in the Central Mediterranean. *Geophysical Journal International*, *145*(3), 809–820. https://doi.org/10.1046/j.0956-540x.2001.01435.x

Faccenna, C., Speranza, F., Caracciolo, F. D. A., Mattei, M., & Oggiano, G. (2002). Extensional tectonics on Sardinia (Italy): Insights into the arc–back-arc transitional regime. *Tectonophysics*, *356*(4), 213–232. https://doi.org/10.1016/s0040-1951(02)00287-1

Filigheddu, R., & Oggiano, G. (1984). Contributo alla stratigrafia delle bauxiti del Cretaceo della Nurra mediante lo studio di un livello pollinico. *Atti della Società Toscana di Scienze Naturali Serie A*, *91*, 111–118.

Fisher, R. A. (1953). Dispersion on a sphere. *Proceedings of the Royal Society of London. Series A. Mathematical and Physical Sciences*, *217*(1130), 295–305. https://doi.org/10.1098/rspa.1953.0064

Gattacceca, J., Deino, A., Rizzo, R., Jones, D. S., Henry, B., Beaudoin, B., & Vadeboin, F. (2007). Miocene rotation of Sardinia: New paleomagnetic and geochronological constraints and geodynamic implications. *Earth and Planetary Science Letters*, *258*(3–4), 359–377. https://doi.org/10.1016/j.epsl.2007.02.003

Gong, Z., Langereis, C. G., & Mullender, T. A. T. (2008). The rotation of Iberia during the Aptian and the opening of the Bay of Biscay. *Earth and Planetary Science Letters*, *273*(1–2), 80–93. https://doi.org/10.1016/j.epsl.2008.06.016

Handy, M. R., Schmid, S. M., Bousquet, R., Kissling, E., & Bernoulli, D. (2010). Reconciling plate-tectonic reconstructions of Alpine Tethys with the geological–geophysical record of spreading and subduction in the Alps. *Earth-Science Reviews*, *102*(3–4), 121–158. https://doi.org/10.1016/j.earscirev.2010.06.002

Horner, F., & Lowrie, W. (1981). Paleomagnetic evidence from Mesozoic carbonate rocks for the rotation of Sardinia. *Journal of Geophysics*, *49*(1), 11–19.

Jammes, S., Manatschal, G., Lavier, L., & Masini, E. (2009). Tectonosedimentary evolution related to extreme crustal thinning ahead of a propagating ocean: Example of the western Pyrenees. *Tectonics*, *28*(4). https://doi.org/10.1029/2008tc002406

Jiang, Z., Liu, Q., Dekkers, M. J., Tauxe, L., Qin, H., Barrón, V., & Torrent, J. (2015). Acquisition of chemical remanent magnetization during experimental ferrihydrite–hematite conversion in Earth-like magnetic field—Implications for paleomagnetic studies of red beds. *Earth and Planetary Science Letters*, *428*, 1–10. https://doi.org/10.1016/j.epsl.2015.07.024

Jolivet, L., Romagny, A., Gorini, C., Maillard, A., Thinon, I., Couëffé, R., et al. (2020). Fast dismantling of a mountain belt by mantle flow: Late-orogenic evolution of Pyrenees and Liguro-Provençal rifting. *Tectonophysics*, *776*, 228312. https://doi.org/10.1016/j.tecto.2019.228312

Kastens, K., Mascle, J., Auroux, C., Bonatti, E., Broglia, C., Channell, J., et al. (1988). ODP Leg 107 in the Tyrrhenian Sea: Insights into passive margin and back-arc basin evolution. *Geological Society of America Bulletin*, *100*(7), 1140–1156. https://doi.org/10.1130/0016-7606(1988)100<1140:olitts>2.3.co;2

King, M. T., Welford, J. K., & Tugend, J. (2023). The role of the Ebro Block on the deformation experienced within the Pyrenean realm: Insights from deformable plate tectonic models. *Journal of Geodynamics*, *155*, 101962. https://doi.org/10.1016/j.jog.2023.101962

Kirscher, U., Aubele, K., Muttoni, G., Ronchi, A., & Bachtadse, V. (2011). Paleomagnetism of Jurassic carbonate rocks from Sardinia: No indication of post-Jurassic internal block rotations. *Journal of Geophysical Research*, *116*(B12), B12107. https://doi.org/10.1029/2011jb008422

Kirschvink, J. L. (1980). The least-squares line and plane and the analysis of palaeomagnetic data. *Geophysical Journal International*, *62*(3), 699–718. https://doi.org/10.1111/j.1365-246x.1980.tb02601.x

Lacombe, O., & Jolivet, L. (2005). Structural and kinematic relationships between Corsica and the Pyrenees-Provence domain at the time of the Pyrenean orogeny. *Tectonics*, *24*(1). https://doi.org/10.1029/2004tc001673

Le Breton, E., Brune, S., Ustaszewski, K., Zahirovic, S., Seton, M., & Müller, R. D. (2021). Kinematics and extent of the Piemont–Liguria Basin–implications for subduction processes in the Alps. *Solid Earth*, *12*(4), 885–913. https://doi.org/10.5194/se-12-885-2021

Lowrie, W. (1990). Identification of ferromagnetic minerals in a rock by coercivity and unblocking temperature properties. *Geophysical Research Letters*, *17*(2), 159–162. https://doi.org/10.1029/gl017i002p00159

Lustrino, M., Morra, V., Fedele, L., & Franciosi, L. (2009). Beginning of the Apennine subduction system in central western Mediterranean: Constraints from Cenozoic "orogenic" magmatic activity of Sardinia, Italy. *Tectonics*, *28*(5). https://doi.org/10.1029/2008tc002419

Maffione, M., Speranza, F., Cascella, A., Longhitano, S. G., & Chiarella, D. (2013). A~ 125 post-early Serravallian counterclockwise rotation of the Gorgoglione formation (Southern Apennines, Italy): New constraints for the formation of the Calabrian Arc. *Tectonophysics*, *590*, 24–37. https://doi.org/10.1016/j.tecto.2013.01.005

Malinverno, A., & Ryan, W. B. (1986). Extension in the Tyrrhenian Sea and shortening in the Apennines as result of arc migration driven by sinking of the lithosphere. *Tectonics*, *5*(2), 227–245. https://doi.org/10.1029/tc005i002p00227

Mameli, P., Mongelli, G., Oggiano, G., & Dinelli, E. (2007). Geological, geochemical and mineralogical features of some bauxite deposits from Nurra (Western Sardinia, Italy): Insights on conditions of formation and parental affinity. *International Journal of Earth Sciences*, *96*(5), 887–902. https://doi.org/10.1007/s00531-006-0142-2

Manzoni, M. (1979). Paleomagnetic evidence for non-Apenninic origin of the Sila nappes (Calabria). *Tectonophysics*, *60*(3–4), 169–188. https://doi.org/10.1016/0040-1951(79)90157-4

Manzoni, M., & Vigliotti, L. (1983). Further paleomagnetic data from northern Calabria: Their bearing on directions of emplacement of the Calabrian nappes. *Bollettino di Geofisica Teorica ed Applicata*, *25*(97), 27–43.

Mattei, M., Cipollari, P., Cosentino, D., Argentieri, A., Rossetti, F., Speranza, F., & Di Bella, L. (2002). The Miocene tectono-sedimentary evolution of the southern Tyrrhenian Sea: Stratigraphy, structural and palaeomagnetic data from the on-shore Amantea basin (Calabrian arc, Italy). *Basin Research*, *14*(2), 147–168. https://doi.org/10.1046/j.1365-2117.2002.00173.x

Mazzoli, S., & Algarra, A. M. (2011). Deformation partitioning during transpressional emplacement of a 'mantle extrusion wedge': The Ronda peridotites, western Betic Cordillera, Spain. *Journal of the Geological Society*, *168*(2), 373–382. https://doi.org/10.1144/0016-76492010-126

McFadden, P. L., & McElhinny, M. W. (1990). Classification of the reversal test in palaeomagnetism. *Geophysical Journal International*, *103*(3), 725–729. https://doi.org/10.1111/j.1365-246x.1990.tb05683.x

Montigny, R., Edel, J. B., & Thuizat, R. (1981). Oligo-Miocene rotation of Sardinia: KAr ages and paleomagnetic data of Tertiary volcanics. *Earth and Planetary Science Letters*, *54*(2), 261–271. https://doi.org/10.1016/0012-821x(81)90009-1

Muttoni, G., Visconti, A., Channell, J. E., Casellato, C. E., Maron, M., & Jadoul, F. (2018). An expanded Tethyan Kimmeridgian magneto-biostratigraphy from the S'Adde section (Sardinia): Implications for the Jurassic timescale. *Palaeogeography, Palaeoclimatology, Palaeoecology*, *503*, 90–101. https://doi.org/10.1016/j.palaeo.2018.04.019

Nairn, A. E. M., & Westphal, M. (1968). Possible implications of the palaeomagnetic study of late Palaeozoic igneous rocks of northwestern Corsica. *Palaeogeography, Palaeoclimatology, Palaeoecology*, *5*(2), 179–204. https://doi.org/10.1016/0031-0182(68)90113-2

Neres, M., Font, E., Miranda, J. M., Camps, P., Terrinha, P., & Mirão, J. (2012). Reconciling Cretaceous paleomagnetic and marine magnetic data for Iberia: New Iberian paleomagnetic poles. *Journal of Geophysical Research*, *117*(B6). https://doi.org/10.1029/2011jb009067

Neres, M., Miranda, J. M., & Font, E. (2013). Testing Iberian kinematics at Jurassic-cretaceous times. *Tectonics*, *32*(5), 1312–1319. https://doi.org/10.1002/tect.20074

Nicolosi, I., Speranza, F., & Chiappini, M. (2006). Ultrafast oceanic spreading of the Marsili Basin, southern Tyrrhenian Sea: Evidence from magnetic anomaly analysis. *Geology*, *34*(9), 717–720. https://doi.org/10.1130/g22555.1

Oggiano, G., Sanna, G., & Temussi, I. (1987). Caracteres geologiques, gitologiques et geochemiques de la bauxite de la Nurra. In A. Cherchi (Ed.), *Livret-Guide excursion en Sardaigne 24–29 Mai 1987* (pp. 72–124). Groupe Francais du Cretace.

Philip, J., & Allemann, J. (1982). Comparaison entre les plates-formes du Crétacé Supérieur deProvence et de Sardaigne. *Cretaceous Research*, *3*(1–2), 35–45. https://doi.org/10.1016/0195-6671(82)90005-2

Pinter, P. R., Butler, R. W., Hartley, A. J., Maniscalco, R., Baldassini, N., & Di Stefano, A. (2018). Tracking sand-fairways through a deformed turbidite system: The Numidian (Miocene) of Central Sicily, Italy. *Basin Research*, *30*(3), 480–501. https://doi.org/10.1111/bre.12261

Rossetti, F., Goffé, B., Monié, P., Faccenna, C., & Vignaroli, G. (2004). Alpine orogenic P-T-t-deformation history of the Catena Costiera area and surrounding regions (Calabrian Arc, southern Italy): The nappe edifice of north Calabria revised with insights on the Tyrrhenian-Apennine system formation. *Tectonics*, *23*(6). https://doi.org/10.1029/2003tc001560

Séranne, M. (1999). The Gulf of Lion continental margin (NW Mediterranean) revisited by IBS: An overview. *Geological Society, London, Special Publications*, *156*(1), 15–36. https://doi.org/10.1144/gsl.sp.1999.156.01.03

Séranne, M., Couëffé, R., Husson, E., Baral, C., & Villard, J. (2021). The transition from Pyrenean shortening to Gulf of Lion rifting in Languedoc (South France)–A tectonic-sedimentation analysis. *BSGF-Earth Sciences Bulletin*, *192*(1), 27. https://doi.org/10.1051/bsgf/2021017

Siravo, G. (2022). Paleomagnetic data from Cixerri Fm. (SW Sardinia) [Dataset]. Zenodo. https://doi.org/10.5281/zenodo.7391331

Siravo, G., Fellin, M. G., Faccenna, C., & Maden, C. (2020). Transpression and the build-up of the Cordillera: The example of the Bucaramanga fault (Eastern Cordillera, Colombia). *Journal of the Geological Society*, *177*(1), 14–30. https://doi.org/10.1144/jgs2019-054

Siravo, G., Speranza, F., & Macrì, P. (2022). First pre-Miocene paleomagnetic data from the Calabrian block document a 160° post-late jurassic CCW rotation as a consequence of left-lateral shear along Alpine Tethys. *Tectonics*, *41*(7), e2021TC007156. https://doi.org/10.1029/2021tc007156

Speranza, F., Hernandez-Moreno, C., Avellone, G., Gasparo Morticelli, M., Agate, M., Sulli, A., & Di Stefano, E. (2018). Understanding paleomagnetic rotations in Sicily: Thrust versus strike-slip tectonics. *Tectonics*, *37*(4), 1138–1158. https://doi.org/10.1002/2017tc004815

Speranza, F., Villa, I. M., Sagnotti, L., Florindo, F., Cosentino, D., Cipollari, P., & Mattei, M. (2002). Age of the Corsica–Sardinia rotation and Liguro–Provençal Basin spreading: New paleomagnetic and Ar/Ar evidence. *Tectonophysics*, *347*(4), 231–251. https://doi.org/10.1016/s0040-1951(02)00031-8

Stampfli, G. M., & Borel, G. D. (2002). A plate tectonic model for the Paleozoic and Mesozoic constrained by dynamic plate boundaries and restored synthetic oceanic isochrons. *Earth and Planetary Science Letters*, *196*(1–2), 17–33. https://doi.org/10.1016/s0012-821x(01)00588-x

Torsvik, T. H., Van der Voo, R., Preeden, U., Mac Niocaill, C., Steinberger, B., Doubrovine, P. V., et al. (2012). Phanerozoic polar wander, palaeogeography and dynamics. *Earth-Science Reviews*, *114*(3–4), 325–368. https://doi.org/10.1016/j.earscirev.2012.06.007

Tugend, J., Manatschal, G., Kusznir, N. J., Masini, E., Mohn, G., & Thinon, I. (2014). Formation and deformation of hyperextended rift systems: Insights from rift domain mapping in the Bay of Biscay-Pyrenees. *Tectonics*, *33*(7), 1239–1276. https://doi.org/10.1002/2014tc003529

Van der Voo, R. (1969). Paleomagnetic evidence for the rotation of the Iberian Peninsula. *Tectonophysics*, *7*(1), 5–56. https://doi.org/10.1016/0040-1951(69)90063-8

van Hinsbergen, D. J., Torsvik, T. H., Schmid, S. M., Maţenco, L. C., Maffione, M., Vissers, R. L., et al. (2020). Orogenic architecture of the Mediterranean region and kinematic reconstruction of its tectonic evolution since the Triassic. *Gondwana Research*, *81*, 79–229. https://doi.org/10.1016/j.gr.2019.07.009

Vigliotti, L., Alvarez, W., & McWilliams, M. (1990). No relative rotation detected between Corsica and Sardinia. *Earth and Planetary Science Letters*, *98*(3–4), 313–318. https://doi.org/10.1016/0012-821x(90)90033-t

Wortmann, U. G., Weissert, H., Funk, H., & Hauck, J. (2001). Alpine plate kinematics revisited: The Adria problem. *Tectonics*, *20*(1), 134–147. https://doi.org/10.1029/2000tc900029

Xypolias, P., Kokkalas, S., & Skourlis, K. (2003). Upward extrusion and subsequent transpression as a possible mechanism for the exhumation of HP/LT rocks in Evia Island (Aegean Sea, Greece). *Journal of Geodynamics*, *35*(3), 303–332. https://doi.org/10.1016/s0264-3707(02)00131-x

Zattin, M., Massari, F., & Dieni, I. (2008). Thermochronological evidence for Mesozoic–Tertiary tectonic evolution in the eastern Sardinia. *Terra Nova*, *20*(6), 469–474. https://doi.org/10.1111/j.1365-3121.2008.00840.x

Zijderveld, J. D. A. (1967). AC demagnetization of rocks: Analysis of results. In *Developments in solid earth geophysics* (Vol. 3, pp. 254–286). Elsevier.

Zijderveld, J. D. A., De Jong, K. A., & Van der Voo, R. (1970). Rotation of Sardinia: Palaeomagnetic evidence from Permian rocks. *Nature*, *226*(5249), 933–934. https://doi.org/10.1038/226933a0